The Astrophysical Journal, 919:71 (12pp), 2021 October 1 https://doi.org/10.3847/1538-4357/ac0c1f

Kinetic Alfvén Waves in Space Plasma Environment with κ-electrons

K. C. Barik, S. V. Singh[1], and G. S. Lakhina
Indian Institute of Geomagnetism Navi Mumbai, 410218, India; kcbarik17@gmail.com, satyavir.s@iigm.res.in
Received 2021 April 1; revised 2021 June 11; accepted 2021 June 11; published 2021 September 28

Abstract

A resonant instability of kinetic Alfvén waves (KAWs) driven by ion beam is discussed through a theoretical model encompassing Maxwellian background ions and beam ions and non-Maxwellian κ-electrons. The ion beam velocity alone as a source is able to excite the KAWs up to a significant growth. The non-Maxwellian parameter κ impedes the growth of KAWs by restricting the wave unstable region. The effects of other plasma parameters such as propagation angle, temperature of the plasma species, and ion plasma beta on the excitation of KAWs are also examined. The present model can generate waves with frequencies in the range of ≈6.6–51.2 mHz, which are relevant to explaining the observed ultralow frequency waves at auroral ionospheric altitudes. Theoretical model predictions will also be applicable to other planetary environments where ion beams and non-Maxwellian κ-electrons are present.

Unified Astronomy Thesaurus concepts: Solar wind (1534); Space plasmas (1544); Alfven waves (23)

1. Introduction

The study of kinetic Alfvén Waves (KAWs) in space plasma physics has drawn much attention since the pioneering work of Hasegawa (1976). Unlike the magnetohydrodynamic (MHD) Alfvén wave, it propagates nearly perpendicular to the ambient magnetic field. KAWs also differ from MHD Alfvén waves, which do not have a parallel component of wave electric field and in which the electrons and ions move together along the field lines. However, when the perpendicular wavelength approaches the ion gyroradius or the electron inertial length the scenario changes. Under such circumstances the ions leave the field lines, whereas the electrons still follow the field lines due to its smaller gyroradius and this happens when the wave dynamics are faster than the ion orbital motion (Gershman et al. 2017). This charge separation produces a parallel electric field that leads to particle energization and auroral acceleration of electrons along the ambient magnetic field (Hui & Seyler 1992; Thompson & Lysak 1996). The polarization and the parallel electric field to transverse magnetic field ratio are important properties of the KAW mode that allow the proper determination of the wave mode. The polarization indicates whether the waves are right-handed KAW or left-handed ion-cyclotron waves (Gary 1986; Narita et al. 2020; Moya et al. 2021). The electric-to-magnetic field ratio gives the phase velocity of the waves, which is helpful in differentiating KAWs from the magnetosonic waves (Hollweg 1999; Salem et al. 2012). Further, these waves are distinguished as kinetic or inertial, depending on the local plasma conditions. When the local Alfvén speed is either greater than the ion thermal speed and less than the electron thermal speed ($V_{\rm the} \gg V_A > V_{\rm thi}$) or it is less than both the ion and electron thermal speeds ($V_A \ll V_{\rm thi}$, $V_{\rm the}$), these waves exist in the kinetic regime (Lysak & Carlson 1981). In both the kinetic limits described above, the electron plasma beta, $\beta_e \gg m_e/m_i$, (m_e/m_i is the ratio of electron-to-ion mass) and the wave parallel electric field is supported by electron pressure gradients. Here, the perpendicular wavelength becomes comparable to the ion gyroradius. These waves are called KAWs (Hasegawa & Chen 1976) and are observed at altitude above 4–5 R_E in Earth's magnetosphere (R_E is the radius of Earth). In the inertial limit (Lysak & Carlson 1981), these waves exist in the cold electron plasma when the local Alfvén speed is greater than both the local electron and ion thermal speeds ($V_A \gg V_{\rm the}$, $V_{\rm thi}$). This corresponds to a condition where $\beta_e \ll m_e/m_i$. Here, wave parallel electric fields are supported by electron inertia (Bellan 2015) and the perpendicular wavelength becomes comparable to the electron inertial length. These waves are called shear kinetic Alfvén waves (Goertz & Boswell 1979) and are observed at altitudes below 4–5 R_E in Earth's magnetosphere. These characteristics of the waves are treated as powerful tools for the identification of waves from the satellite data.

Ion beams and nonthermal particle distributions are found in the solar corona, solar flares, solar wind, and planetary environments (Simnett 1995; Procházka et al. 2018; Zastrow 2016; Delamere et al. 2021). It has been suggested that KAWs excited in the coronal loops can lead to an efficient electron heating (Malara et al. 2019). Observational evidence suggests the existence of ion beams in both fast and slow solar winds (Goldstein et al. 2010). The Mars Atmosphere and Volatile EvolutioN (MAVEN) spacecraft has confirmed the existence of oxygen ion beam on the surface of the red planet Mars (Zastrow 2016). A low plasma beta environment is found in both the solar flare (Iwai et al. 2014) and solar wind (Rathore et al. 2015) as well as in the mid-coronal region (Gary 2001). Simulation studies by Delamere et al. (2021) indicate that the fluctuations of electric and magnetic field show the features of KAWs in the Saturn magnetosphere. The measurements by Cassini/CAPS and the Magnetosphere Imaging Instrument (MIMI) have confirmed the existence of superthermal plasma species in the Saturn magnetosphere (Sergis et al. 2013). Observations by the Nozomi spacecraft and Helios have provided evidence for the presence of nonthermal ions in the vicinity of the Moon (Futaana et al. 2003) and solar wind (Marsch et al. 1982), respectively. Also, nonthermal oxygen ions are found to exist in the Martian ionosphere as evidenced from MAVEN data (Leblanc et al. 2017).

KAWs play a very important role in space plasma dynamics. Theoretical study by Hasegawa (1976) has shown that the

[1] Corresponding author.

hydromagnetic surface waves can covert to KAWs by resonant mode conversion mechanism. It is found that the velocity shear driven KAWs can generate ultralow frequency (ULF) waves in the polar cusp and auroral field lines regions (Lakhina 1990, 2008). KAWs play a crucial role in electron trapping and acceleration in solar flares (Artemyev et al. 2016). The localization and turbulence in space plasmas produced by KAWs is studied through simulation (Sharma & Modi 2013; Sharma et al. 2014). It is also found from a 3D hybrid simulation that KAWs are generated at the reconnection region in the dayside magnetopause and transported to the polar cusp, which may lead to auroral brightening (Wang et al. 2019).

There are ample observational evidences that support the existence of KAWs in space plasma environment. Salem et al. (2012) have reported that the small-scale turbulent fluctuations found in the solar wind have the characteristics similar to KAWs. They reached this conclusion by comparing the electric and magnetic field data of the Cluster spacecraft with that of a theoretical model. KAWs are also excited at the substorm onset due to the gradient in number density and magnetic field and thereby trigger the substorm expansion phase as observed at the near Earth plasma sheet (NEPS; Duan et al. 2012). Chaston et al. (2012) using the Time History of Events and Macroscale Interactions during Substorms (THEMIS) data found that the wave field fluctuations having frequency $f_{sc} \approx (0.2–20)$ Hz in the spacecraft frame are well explained by KAWs. The strong perpendicular electric field (with respect to the ambient magnetic field) of the KAWs energizes the O^+ ions of the polar cusp/ionospheric origin and transfers them from the lobe to the plasma sheet region during intensification of substorm dipolarization as confirmed by the study of the Cluster mission (Duan et al. 2017). Using magnetospheric multiscale data Gershman et al. (2017) verified the wave-particle energy exchange between the undamped KAW field and plasma particles. The Van Allen probes studies showed that the wave fields of the broad κ-spectrum of kinetic Alfvén waves are responsible for radiation belt electron depletions during the storm main phase (Chaston et al. 2018). Observational evidence from the Viking, Freja (Louarn et al. 1994), and the Fast Auroral SnapshoT (FAST) spacecraft, as well as low altitude sounding rockets (Boehm et al. 1990) confirmed that KAWs in the inertial limit are an important features at altitude from 1000 km to 2.5 R_E. It is found from the study of POLAR spacecraft data (Wygant et al. 2002) that the intense KAWs play a crucial role in creating the field aligned electron distribution function and parallel acceleration of electrons that are able to explain the ionospheric auroral phenomena. KAWs are also generated during the interplanetary shock-induced geomagnetic storm (Moya et al. 2015).

ULF waves have been detected in different regions of Earth's magnetosphere such as magnetopause (Johnson et al. 2001; Chaston et al. 2005), auroral region (Boehm et al. 1990; Louarn et al. 1994; Wahlund et al. 1994), magnetotail, plasma sheet boundary layer (PSBL; Keiling et al. 2000, 2002, 2005; Wygant et al. 2002; Duan et al. 2012), central plasma sheet (Keiling et al. 2001), and NEPS (Duan et al. 2012) etc. These are the thick transition regions that contain a gradient in velocity called velocity shear, which is considered as a source of free energies for many space plasma dynamics. Ion beam is also observed in different magnetospheric regions such as PSBL (Parks et al. 1998; Takada et al. 2005), polar cusp (Grison et al. 2005), bow shock (Meziane et al. 2007), auroral zone (Schriver et al. 1990), etc. Many theories such as MHD surface waves, Kelvin–Helmholtz instabilities etc. have been proposed so far to explain the generation mechanisms of these ULF waves in Earth's magnetosphere (D'Angelo 1973, 1977; Chen & Hasegawa 1974; Hasegawa 1976; Hasegawa & Chen 1976; Hasegawa & Mima 1978; Goertz & Boswell 1979; Huba 1981; Lysak & Dum 1983; Lakhina 1987, 1990; Lysak & Lotko 1996; Thompson & Lysak 1996; Nosé et al. 1998). Theoretical studies have shown that the excitation of KAWs in different magnetospheric regions is able to explain the observed characteristics of these ULF waves. Lakhina (2008) studied the generation of KAWs by velocity shear through resonant and nonresonant instabilities and found that the frequency of KAWs in the spacecraft frame is in the range of ULF waves. This study has been extended further by Barik et al. (2019a, 2019b) to see the combined effects of ion beam and velocity shear on the generation of KAWs and found that presence of the both acts as a dual source for the excitation of KAWs and can produce higher wave growth rates as compared to the individual source of ion beam and velocity shear. They also reported that antiparallel streaming (with respect to the ambient magnetic field) ion beam and positive velocity shear creates favorable conditions for wave excitation with larger growth rates. However, these studies are based on the Maxwellian distribution function, whereas satellite observations have shown that the space plasma populations are well fitted by a distribution having a long energy tail and best described by a non-Maxwellian distribution, such as a κ-distribution (Vasyliunas 1968; Pierrard & Lazar 2010; Livadiotis 2015; Lazar et al. 2016). In the presence of κ-electrons, resonant instability of the KAWs generated by velocity shear has been examined by Barik et al. (2019c). It was found that the κ-electron impedes the growth rate of KAWs by restricting the wave unstable region. The nonresonant instability of KAWs by ion beam and velocity shear in the presence of κ-electrons is carried out by Barik et al. (2020). Here, we propose a three-component theoretical plasma model consisting of κ-electrons, ion beam, and background ions to study the generation of KAWs. The background ions and ion beam are considered Maxwellian. The KAWs are generated by an ion beam through resonant instability. The paper is organized as follows. A theoretical model is presented in Section 2. A dispersion relation is derived in Section 3 and the resonant instability of KAWs driven by ion beam is discussed in Section 4. The numerical results are analyzed in Section 5 followed by a discussion and conclusions in Section 6.

2. Theoretical Model

We consider a three-component plasma that encompasses background ions (N_i, T_i) and beam ions (N_B, T_B, V_B) having Maxwellian and drifting Maxwellian distributions, respectively, and electrons (N_e, T_e) having κ-distribution as its constituents. Here, N_j, T_j, and V_j are the number density, temperature, and beam velocity of the jth species, respectively. Further, $j = i$, e, and B stands for background ions, electrons, and beam ions, respectively. In the equilibrium state the quasi-neutrality is satisfied by the condition, $N_e = N_i + N_B$. In this model the ambient magnetic field $\boldsymbol{B}_0$ is along the z-direction. The wave electric field and the propagation vector $\boldsymbol{k}$ are in the yz-plane.

The distribution functions for background ions, beam ions, and κ-electrons are given by Maxwellian for background ions

$$f_{0i}(v) = \frac{N_i}{\sqrt{\pi^3}\,\alpha_i^3}\exp\left(-\frac{v^2}{\alpha_i^2}\right), \quad (1)$$

drifting Maxwellian for beam ions

$$f_{0B}(v_\perp, v_\parallel) = \frac{N_B}{\sqrt{\pi^3}\,\alpha_B^3}\exp\left[-(v_\perp^2 + (v_\parallel - V_B)^2)/\alpha_B^2\right], \quad (2)$$

and κ-distribution for electrons (Summers et al. 1994)

$$f_{oe}(v) = \frac{N_e}{\pi^{3/2}\Theta_e^3}\frac{\Gamma(\kappa+1)}{\kappa^{3/2}\Gamma(\kappa-1/2)}\left(1+\frac{v^2}{\kappa\Theta_e^2}\right)^{-(\kappa+1)}. \quad (3)$$

Here, Γ represents the gamma function. The parameter κ is reciprocally related to the non-Maxwellian property, i.e., smaller κ indicates highly non-Maxwellian electrons and vice versa. The generalized thermal speed of electron Θ_e is related to the normal thermal speed $\alpha_e = \left(\frac{2T_e}{m_e}\right)^{1/2}$ by the relation

$$\Theta_e = \left[\left(\frac{\kappa-3/2}{\kappa}\right)\right]^{1/2}\left(\frac{2T_e}{m_e}\right)^{1/2} = \left[\left(\frac{\kappa-3/2}{\kappa}\right)\right]^{1/2}\alpha_e. \quad (4)$$

It is to be noted that Equation (3) is valid for $\kappa > 3/2$ as below this value the expression for Θ_e (Equation (4)) is not physical.

Here, V_B represents the uniform drifting of the beam ion along the ambient magnetic field, i.e., z-direction, $\alpha_i = \left(\frac{2Ti}{m_i}\right)^{1/2}$ and $\alpha_B = \left(\frac{2T_B}{m_B}\right)^{1/2}$ are the thermal speed of the background ions and beam ions, respectively. Also, m_i, m_e, and m_B indicate the mass of background ions, electrons, and beam ions, respectively.

Since we are considering low beta plasma (the ratio of thermal to magnetic pressure), the incompressibility of the perturbed magnetic field along the ambient magnetic field direction allows us to write the wave electric field as the gradient of two different scalar potentials, i.e., ψ along the parallel direction and ϕ along the perpendicular direction (Hasegawa 1976)

$$\boldsymbol{E} = E_\perp\hat{y} + E_\parallel\hat{z} = -\boldsymbol{\nabla}_\perp\phi - \boldsymbol{\nabla}_\parallel\psi, \quad (5)$$

where $E_\perp = -\nabla_\perp\phi$ and $E_\parallel = -\nabla_\parallel\psi$ are the perpendicular and parallel components of the wave electric field, respectively.

Vlasov's equation is used to find the perturbed distribution function. Under the plane wave approximation, a perturbation of the form $f_{1j} = \exp(ik_\perp y + ik_\parallel z - i\omega t)$ is assumed, where $k_\perp$ and $k_\parallel$ are the perpendicular and parallel components of the propagation vector $\boldsymbol{k}$, respectively, and ω is frequency of the wave. Thus, the perturbed distribution function is given by Lakhina (2008); Barik et al. (2019a)

$$f_{1j} = \frac{e_j}{m_j}\sum_{n=-\infty}^{+\infty}\sum_{m=-\infty}^{+\infty}\frac{e^{i(n-m)\theta}}{(k_\parallel v_z - \omega + n\omega_{cj})} \times J_n(\xi_j)J_m(\xi_j) \times (k_\perp M_j\phi + k_\parallel L_j\psi), \quad (6)$$

where coefficients M_j and L_j can be expressed as (Lakhina 2008; Barik et al. 2019a)

$$M_j = \left(1 - \frac{k_\parallel v_z}{\omega}\right)\left[\frac{\partial f_{0j}}{\partial v_\perp}\cdot\frac{n\omega_{cj}}{k_\perp v_\perp}\right] + \frac{\partial f_{0j}}{\partial v_z}\frac{n\omega_{cj}}{\omega}\frac{k_\parallel}{k_\perp}, \quad (7)$$

$$L_j = \frac{k_\perp v_z}{\omega}\left[\frac{\partial f_{0j}}{\partial v_\perp}\cdot\frac{n\omega_{cj}}{k_\perp v_\perp}\right] + \left(1 - \frac{n\omega_{cj}}{\omega}\right)\frac{\partial f_{0j}}{\partial v_z}. \quad (8)$$

Here, $J_n(\xi_j)$ and $J_m(\xi_j)$ are the Bessel function of order n and m, respectively, with $\xi_j = \left(\frac{k_\perp v_\perp}{\omega_{cj}}\right)$. Also, $\omega_{cj} = \left(\frac{e_j B_0}{cm_j}\right)$ is the cyclotron frequency of the plasma species j and e_j and m_j represents the charge and mass of the plasma species j, respectively, and c is the speed of light.

The perturbed number density n_j and the z-component of current density J_{zj} are obtained by substituting f_{1j} from Equation (6) into the following expressions:

$$n_j = \int d^3v f_{1j}, \quad J_{zj} = \int d^3v e_j v_z f_{1j}. \quad (9)$$

Here, a cylindrical coordinate system $(v_\perp, \theta, v_\parallel)$ is used and $\int d^3v = \int_0^\infty v_\perp dv_\perp \int_{-\infty}^\infty dv_\parallel \int_0^{2\pi} d\theta$. Using Equations (1)–(3) in Equation (6) perturbed distribution functions are obtained for background ions, beam ions, and electrons, respectively. Further, the perturbed number densities and z-component of current densities for background ions, beam ions, and electrons are obtained from Equations (6) and (9) and are given as follows: for background ions

$$n_i = \frac{N_i e}{m_i}\frac{2}{\alpha_i^2}\left\{[(1-b_i)]\phi + \left[b_i Z'\left(\frac{\omega}{k_\parallel\alpha_i}\right)\right]\psi\right\}, \quad (10)$$

$$J_{zi} = \frac{N_i e^2}{m_i}\left\{\frac{\omega}{k_\parallel\alpha_i^2}b_i Z'\left(\frac{\omega}{k_\parallel\alpha_i}\right)\right\}\psi; \quad (11)$$

for beam ions

$$n_B = \frac{N_B e}{m_B}\left\{\left[\frac{2}{\alpha_B^2}\frac{\bar{\omega}}{\omega}(1-b_B)\right]\phi + \left[\frac{b_B}{\alpha_B^2}Z'\left(\frac{\bar{\omega}}{k_\parallel\alpha_B}\right)\right]\psi\right\}, \quad (12)$$

$$J_{zB} = \frac{N_B e^2}{m_B}\left[\frac{\omega}{k_\parallel\alpha_B^2}b_B Z'\left(\frac{\bar{\omega}}{k_\parallel\alpha_B}\right)\right]\psi; \quad (13)$$

for κ-electrons

$$n_e = \frac{N_e e}{m_e}\left\{\left[-\left(\frac{\kappa-1}{\kappa}\right)^{1/2}\frac{1}{\omega_{ce}^2}\right]\phi + \left[\frac{1}{k_\parallel^2\Theta_e^2} \times \left\{\frac{(2\kappa-1)}{\kappa} + \frac{i\sqrt{\pi}\,\kappa!}{\kappa^{3/2}\Gamma(\kappa-1/2)}\left(\frac{2\omega}{k_\parallel\Theta_e}\right)\right\}\right]\psi\right\}, \quad (14)$$

$$J_{ze} = \frac{N_e e^2}{m_e}\frac{\omega}{k_\parallel\Theta_e^2}\left\{\frac{(2\kappa-1)}{\kappa} + \frac{i\sqrt{\pi}\,\kappa!}{\kappa^{3/2}\Gamma(\kappa-1/2)}\frac{2\omega}{k_\parallel\Theta_e}\right\}\psi. \quad (15)$$

The details of the algebraic steps to arrive at perturbed number and current densities of κ-electrons are provided in the Appendix.

These perturbed densities, i.e., n_j and J_{zj} are further used in the Poisson's equation and z-component of Ampere's law given below.

Poisson's equation:

$$-\nabla_\perp^2\phi - \nabla_\parallel^2\psi = 4\pi\sum_j e_j n_j. \tag{16}$$

The z-component of Ampere's law:

$$\frac{\partial\nabla_\perp^2\phi}{\partial z} - \frac{\partial\nabla_\perp^2\psi}{\partial z} = \frac{4\pi}{c^2}\frac{\partial}{\partial t}\sum_j J_{zj}. \tag{17}$$

Further simplification of Equations (16) and (17) and rearranging the coefficients of ψ and ϕ, we obtain the following relation:

$$\begin{bmatrix} D_{11} & D_{12} \\ D_{21} & D_{22} \end{bmatrix}\begin{bmatrix} \phi \\ \psi \end{bmatrix} = 0, \tag{18}$$

where the coefficients of ψ and ϕ are given by

$$D_{11} = k_\perp^2\Bigg[1 + \left(\frac{\kappa-1}{\kappa}\right)^{1/2}\left(\frac{\omega_{pe}^2}{\omega_{ce}^2}\right) + \frac{2\omega_{pi}^2}{k_\perp^2\alpha_i^2}(1-b_i) + \frac{2\omega_{pB}^2}{k_\perp^2\alpha_B^2}\frac{\bar\omega}{\omega}(1-b_B)\Bigg], \tag{19}$$

$$D_{12} = k_\parallel^2\Bigg[1 + \frac{\omega_{pe}^2}{k_\parallel^2\Theta_e^2}\Bigg\{\frac{(2\kappa-1)}{\kappa} + \frac{i\sqrt{\pi}\,\kappa!}{\kappa^{3/2}\Gamma(\kappa-1/2)} \times\left(\frac{2\omega}{k_\parallel\Theta_e}\right)\Bigg\} - \frac{\omega_{pi}^2}{k_\parallel^2\alpha_i^2}b_i Z'\left(\frac{\omega}{k_\parallel\alpha_i}\right) - \frac{\omega_{pB}^2}{k_\parallel^2\alpha_B^2}b_B Z'\left(\frac{\bar\omega}{k_\parallel\alpha_B}\right)\Bigg], \tag{20}$$

$$D_{21} = k_\parallel k_\perp^2, \tag{21}$$

$$D_{22} = -k_\parallel k_\perp^2\Bigg[1 - \frac{\omega_{pe}^2}{c^2k_\perp^2}\Bigg\{\frac{(2\kappa-1)}{\kappa}\frac{\omega^2}{k_\parallel^2\Theta_e^2} + \frac{i\sqrt{\pi}\,\kappa!}{\kappa^{3/2}\Gamma(\kappa-1/2)}\frac{2\omega^3}{k_\parallel^3\Theta_e^3}\Bigg\} + \frac{\omega_{pi}^2}{c^2k_\perp^2}\Bigg\{\frac{\omega^2}{k_\parallel^2\alpha_i^2}b_i Z'\left(\frac{\omega}{k_\parallel\alpha_i}\right)\Bigg\} + \frac{\omega_{pB}^2}{c^2k_\perp^2}\Bigg\{\frac{\omega^2}{k_\parallel^2\alpha_B^2}b_B Z'\left(\frac{\bar\omega}{k_\parallel\alpha_B}\right)\Bigg\}\Bigg]. \tag{22}$$

Here, $\omega_{pj} = \left(\frac{4\pi N_j e_j^2}{m_j}\right)^{1/2}$ is the plasma frequency of species j, $\bar\omega = (\omega - k_\parallel V_B)$ is the Doppler shifted frequency of beam ion. Further, $b_{i,B} = I_0(\lambda_{i,B})\exp(-\lambda_{i,B})$ are the zeroth order modified Bessel function with $\lambda_{i,B} = \left(\frac{k_\perp^2\alpha_{i,B}^2}{2\omega_{ci,B}^2}\right)$, $Z\left(\frac{\bar\omega}{k_\parallel\alpha_B}\right)$ is the plasma dispersion function and $Z'\left(\frac{\bar\omega}{k_\parallel\alpha_B}\right)$ is the derivative w.r.t. its argument. It is worth mentioning that the electron terms that are contained in the coefficients given by Equations (19)–(22) are obtained by expanding $\lambda_e \ll 1$ limit and retaining leading order terms and by the expansion of modified plasma dispersion function (Summers et al. 1994) for electrons in the limit $\frac{\omega^2}{k_\parallel^2\alpha_e^2} \ll 1$ that is satisfied for hot electrons. Furthermore, to obtain Equations (19)–(22), we have made the assumptions of $\omega \ll \omega_{cj}$ and $k_\parallel \ll k_\perp$, i.e., low frequency electromagnetic waves propagating nearly perpendicular to the ambient magnetic field. The mathematical steps for the derivation of the above expressions are provided in the Appendix. The present theoretical work on KAWs involving κ-distribution is carried out analytically; however, a few authors (Gaelzer & Ziebell 2014; Astfalk et al. 2015; López et al. 2019) have studied other plasma waves and instabilities numerically involving κ-distributions.

3. Dispersion Relation

The dispersion relation of the KAW is obtained by equating the determinant of the coefficients of ϕ and ψ to zero in Equation (18) and is given by

$$\frac{b_i N_i}{N_e}\left[1 - \frac{\omega^2}{k_\parallel^2 v_A^2}\frac{N_i}{N_e}\frac{1-b_i}{\lambda_i}A\right] - \frac{\omega^2}{k_\parallel^2 c_s^2}\left[C_R' + iC_I - \frac{\omega^2}{k_\parallel^2 v_A^2}\frac{N_i}{N_e}\frac{1-b_i}{\lambda_i}A(C_R + iC_I)\right] = \frac{2\omega^2}{k_\parallel^2\alpha_i^2}\frac{(1-b_i)N_i}{N_e}, \tag{23}$$

where

$$A = 1 + \frac{N_B}{N_i}\frac{T_i}{T_B}\frac{\bar\omega}{\omega}\frac{(1-b_B)}{(1-b_i)}, \tag{24}$$

$$C_R = \frac{(2\kappa-1)}{(2\kappa-3)} + \frac{N_B}{N_e}\frac{T_e}{T_B}b_B, \tag{25}$$

$$C_R' = \frac{(2\kappa-1)}{(2\kappa-3)} + \frac{N_B}{N_e}\frac{T_e}{T_B}\left\{b_B\left(1 - \frac{\bar\omega}{\omega}\right) + \frac{\bar\omega}{\omega}\right\}, \tag{26}$$

$$C_I = \sqrt{\pi}\frac{\omega}{k_\parallel\theta_e}\Bigg[\frac{\kappa!}{\kappa^{3/2}\Gamma(\kappa-1/2)}\frac{2\kappa}{(2\kappa-3)} + b_B\frac{N_B}{N_e} \times\left(\frac{T_e}{T_B}\right)^{3/2}\left(\frac{m_B}{m_e}\right)^{1/2}\frac{\bar\omega}{\omega} \times\left(\frac{2\kappa-3}{2\kappa}\right)^{1/2}\exp\left(-\frac{\bar\omega^2}{k_\parallel^2\alpha_B^2}\right)\Bigg]. \tag{27}$$

Here, $v_A = \frac{B_0}{\sqrt{4\pi N_e m_i}}$ is the Alfvén speed, $\beta_i = (8\pi N_e T_i/B_0^2)$ and $\beta_B = (8\pi N_e T_B/B_0^2)$ are the ion and beam plasma betas, respectively and $c_s = \left(\frac{T_e}{m_i}\right)^{1/2}$ is the ion acoustic speed. Further, C_I contains terms due to electrons and beam ions. While arriving at Equation (23) the plasma dispersion function is expanded in the limit $\frac{\omega^2}{k_\parallel^2\alpha_i^2} \gg 1$ for background ions, which is cold and $\frac{\omega^2}{k_\parallel^2\alpha_B^2} \ll 1$ for hot beam ions.

The result for a two component electron-ion plasma (where beam ions are not present, i.e., $N_B = 0$) is obtained by

neglecting the damping term in Equation (23) as

$$\left[b_i - \frac{(2\kappa - 1)}{(2\kappa - 3)}\frac{\omega^2}{k_\parallel^2 c_s^2}\right]\cdot\left[1 - \frac{\omega^2}{k_\parallel^2 v_A^2}\frac{1 - b_i}{\lambda_i}\right] = \frac{2\omega^2(1 - b_i)}{k_\parallel^2 \alpha_i^2}. \quad (28)$$

Equation (28) shows the coupling between two different wave eigenmodes, i.e., the KAW and ion acoustic wave (IAW) mode in the presence of κ-electrons. This expression resembles to Equation (36) of Hasegawa & Chen (1976) and Equation (23) of Lakhina (2008) in the limit $\kappa \to \infty$ that describes the coupling in the presence of Maxwellian electrons. In the low plasma beta limit, i.e., $\beta_i \ll 1$ the coupling between KAWs and IAWs becomes weak and two distinct wave modes are obtained (see Equations (27) and (28) of Barik et al. 2019c) for κ-electrons and Equations (24) and (25) of Lakhina (2008) in the limit $\kappa \to \infty$ i.e., for Maxwellian electrons. The expressions for decoupled KAW and IAW modes for κ-electrons are given below.

For Kinetic Alfvén wave

$$\omega^2 \approx k_\parallel^2 v_A^2\left[\frac{\lambda_i}{(1 - b_i)} + \frac{(2\kappa - 3)}{(2\kappa - 1)}\frac{T_e}{T_i}\lambda_i\right] \quad (29)$$

and for the ion acoustic wave

$$\omega^2 \approx b_i k_\parallel^2 c_s^2\left[\frac{(2\kappa - 1)}{(2\kappa - 3)} + \frac{T_e(1 - b_i)}{T_i}\right]^{-1}. \quad (30)$$

The result of coupling between KAWs and IAWs has been explained numerically by Barik et al. (2020) in a very detailed manner for both Maxwellian and κ-electrons.

4. KAW Resonant Instability by Ion Beam

The resonant instability of KAWs generated by ion beam is studied by analyzing Equation (23), which can be written in terms of real and imaginary parts as

$$D_R(\omega, k) + iD_I(\omega, k) = 0, \quad (31)$$

where the real and imaginary parts are given by

$$D_R(\omega, k) = \frac{\omega^4}{k_\parallel^4 v_A^4}\left[\frac{N_i}{N_e}\frac{(1 - b_i)}{\lambda_i}AC_R\right] - \mathrm{g}_1\frac{\omega^2}{k_\parallel^2 v_A^2} + \frac{N_i}{N_e}\frac{b_i\beta_i}{2}\frac{T_e}{T_i}, \quad (32)$$

$$D_I(\omega, k) = -\frac{\omega^2}{k_\parallel^2 v_A^2}\left[1 - \frac{\omega^2}{k_\parallel^2 v_A^2}\frac{(1 - b_i)}{\lambda_i}\frac{N_i}{N_e}A\right]C_I, \quad (33)$$

$$\mathrm{g}_1 = \left[C_R' + \frac{N_i}{N_e}(1 - b_i)\frac{T_e}{T_i}\left\{1 + \frac{N_i}{N_e}\frac{b_i\beta_i}{2\lambda_i}A\right\}\right]. \quad (34)$$

The solution of $D_R(\omega, k) = 0$ provides the expression of real frequency as

$$\omega^2 = \frac{k_\parallel^2 v_A^2}{2}\frac{\lambda_i N_e}{(1 - b_i)AN_iC_R}[\mathrm{g}_1 \pm (\mathrm{g}_1^2 - 4\mathrm{g}_0)^{1/2}], \quad (35)$$

$$\mathrm{g}_0 = \left(\frac{N_i}{N_e}\right)^2\frac{b_i\beta_i}{2}\frac{T_e}{T_i}\frac{(1 - b_i)}{\lambda_i}AC_R. \quad (36)$$

The growth/damping rate of the KAWs is given by

$$\gamma = -\frac{D_I(\omega_r, k)}{\frac{\partial D_R(\omega_r, k)}{\partial \omega_r}} = \frac{\omega_r^2\left[1 - \frac{\omega_r^2}{k_\parallel^2 v_A^2}\frac{(1 - b_i)}{\lambda_i}\frac{N_i}{N_e}A\right]C_I}{\omega_r[2(\mathrm{g}_1^2 - 4\mathrm{g}_0)^{1/2}] + k_\parallel V_B\frac{N_B}{N_e}(1 - b_B)\left[\frac{\omega_r^2}{k_\parallel^2 v_A^2}\frac{T_i}{T_B}\frac{C_R}{\lambda_i} - \frac{T_e}{T_B}\left(1 + \frac{N_i}{N_e}\frac{b_i\beta_i}{2\lambda_i}\right)\right]} \quad (37)$$

The normalized real frequency obtained from Equation (35) and growth rate from Equation (37) are plotted for the numerical analysis in the section below. For the computational purposes, the plasma parameters are normalized as follows: the real frequency (ω_r) and growth rate (γ) are normalized with respect to the beam ion-cyclotron frequency (ω_{cB}), the electron (T_e, N_e) and ion (T_i, N_i) temperatures and number density by the beam ion temperature (T_B) and number density (N_e), respectively, and the drifting speed of beam ion (V_B) with the thermal speed of the beam ion (α_B). The numerical analysis reveals that KAWs have positive growth rate when $C_R > 0$ and $C_I < 0$.

5. Numerical Analysis

For numerical computations, the plasma parameters relevant to the auroral field lines/polar cusp region at an altitude of 5–7 R_E are considered. The representative plasma parameters used are as follows: ion beam densities $N_B/N_e = 0.01-0.2$, ion beam speed $V_B/\alpha_B < 2$, $\beta_i = 0.001$–0.05, ion beam cyclotron frequency $\omega_{CB}/2\pi = (2.2$–$3.0)$ Hz, hot electron temperature, $T_e = 100$ eV, the background cold ion temperature, $T_i = 10$ eV, and beam ion temperature, $T_B = 1$–2 keV (D'Angelo et al. 1974; Gurnett & Frank 1978; Lysak & Lotko 1996; Wygant et al. 2005; Takada et al. 2005; Lakhina 2008; Barik et al. 2019a). It is important to mention here that the normalized real frequencies (Figure 1(a)) and linear growth rates (Figure 1(b)) in all the figures have been plotted for the λ_B range for which all the approximations considered, i.e., cold background ions ($\omega \gg k_\parallel\alpha_i$), hot electrons ($\omega \ll k_\parallel\alpha_e$), and hot beam ions ($\bar{\omega} \leqslant k_\parallel\alpha_B$) are satisfied. Therefore, curves (real frequency and growth rates) are truncated for the range of λ_B where the above mentioned conditions are not satisfied.

The ion beam is treated as one of the free energy sources for the generation of different wave instabilities in Earth's magnetosphere. The variation of normalized real frequency and growth rate with the square of the normalized perpendicular wavenumber λ_B for both Maxwellian and non-Maxwellian electrons for different values of ion beam velocity are depicted in Figure 1. For κ-electrons, the growth rate increases significantly with the increase in ion beam velocity V_B/α_B, while the change in real frequency is negligible although the wave unstable region (i.e., the range of λ_B for which the growth rate is positive) increases for both the real frequency and growth rate as well. The value of λ_B corresponding to the maximum growth rate is referred to as $\lambda_{B\,\max}$. For κ-electrons it can be seen that with the increase in ion beam velocity the $\lambda_{B\,\max}$ shifts toward higher λ_B. For the same value of ion beam velocity ($V_B/\alpha_B = 0.7$ here), a comparison is made between the Maxwellian and non-Maxwellian electrons. It is found that the

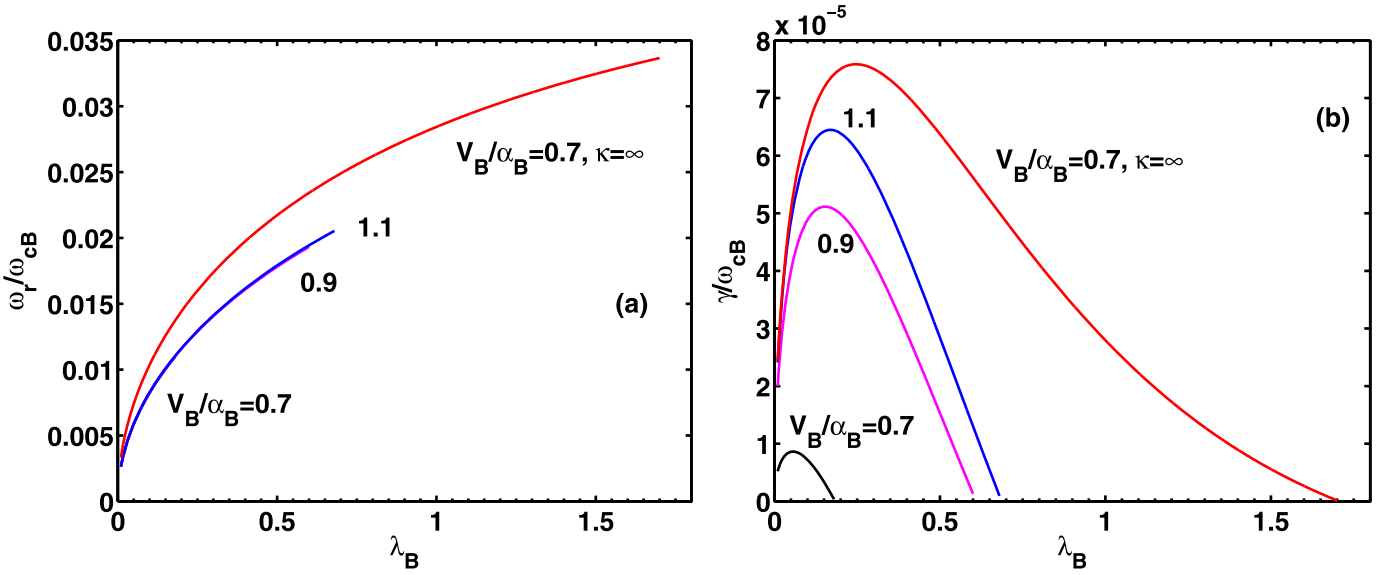

Figure 1. KAWs' resonant instability driven by ion beam: variation of (a) normalized real frequency, ω_r/ω_{cB}, and (b) normalized growth rate, γ/ω_{cB} vs. $\lambda_B = \frac{k_\perp^2 \alpha_B^2}{2\omega_{cB}^2}$ for $\frac{N_B}{N_e} = 0.18$, $\beta_i = 0.001$, $\theta = 87.14°$, $T_i/T_B = 0.016$, $T_e/T_B = 0.6$, and various values of V_B/α_B as listed on the curves. All the curves are plotted for $\kappa = 3$ except the one which is for $\kappa = \infty$ as mentioned on the curve.

Table 1

Shows the Threshold and Upper Values of Ion Beam Velocity, Maximum Growth Rate and Corresponding Ion Beam Velocity at Different Values of κ for Plasma Parameters $\frac{N_B}{N_e} = 0.18$, $\beta_i = 0.001$, $\theta = 87.14°$, $T_i/T_B = 0.016$, $T_e/T_B = 0.6$

κ-parameter	Threshold Value of V_B/α_B	Upper Value of V_B/α_B	Maximum Growth Rate γ_{max}/ω_{cB}	V_B/α_B Value Corresponding to Maximum Growth
3	0.651	1.63	6.4702×10^{-5}	1.078
4	0.622	1.778	1.2083×10^{-4}	1.11
5	0.613	1.846	1.5571×10^{-4}	1.124
∞	0.606	2.04	2.9092×10^{-4}	1.173

Maxwellian electrons can produce a larger growth rate and real frequency as compared to the non-Maxwellian electron and also enhance the wave unstable region for the same value of ion beam velocity. From the numerics, it is observed that the growth rate of the KAWs for κ-electrons starts at a threshold value of the ion beam velocity ($V_B/\alpha_B = 0.651$ for the plasma parameters considered here), reaches the maximum at a certain value (for $V_B/\alpha_B = 1.078$), and then starts decreasing and there is no growth beyond $V_B/\alpha_B = 1.63$. It is clearly noticeable that the wave growth rate increases with the increase in ion beam velocity that leads to the enhancement in KAW power, which confirms the prediction of Hong et al. (2012). Table 1 shows the variation of the ion beam velocity threshold value for κ- to Maxwellian electrons. It is found that the threshold value of the ion beam velocity increases with the decrease in the value of the κ-parameter, i.e., the presence of a highly non-Maxwellian electron requires a higher threshold, whereas the wave can be excited by a comparatively smaller threshold value when Maxwellian electrons are present. It is also noticed that the upper value beyond which there is no growth decreases with the decrease in κ-parameter. Hence, it can be concluded that the range of ion beam velocity (V_B/α_B) over which the growth of the KAW is obtained enhances as the κ-electron approaches the Maxwellian electron. For the sake of clarity, it is important to mention that the parameter κ represents the non-Maxwellian properties of the distribution function of the plasma species. The smaller value, say $\kappa = 2$–6 represents a highly non-Maxwellian distribution and $\kappa = \infty$ represents a Maxwellian distribution.

The non-Maxwellian κ-parameter plays a very crucial role in explaining some of the observed phenomena in space plasma physics as its presence may facilitate the growth/stability of the waves. The effect of non-Maxwellian parameter κ on the real frequency and growth rate of KAWs at a fixed ion beam velocity ($V_B/\alpha_B = 1.0$ here) is delineated in Figure 2. For a highly non-Maxwellian electron ($\kappa = 2$ here), there is no growth, only damping of the wave is seen. It is because the present plasma parameters are unable to provide the threshold energy required for the excitation of KAWs. However, with such plasma parameters if the T_e/T_B value is raised to 0.71, the KAWs with positive growth rates are excited for $\kappa = 2$ as well. With the increase in non-Maxwellian parameter κ both the real frequency and growth rate increase along with the increase in wave unstable region and also the maximum real frequency and growth rate are obtained for Maxwellian electrons. The $\lambda_{B\,max}$ shifts toward the higher λ_B region as the κ-parameter approaches the Maxwellian. From the above analysis, it can be concluded that the presence of κ-electrons impedes the growth rate of KAWs and restricts the wave unstable region when ion beam velocity is considered as one of the free energy sources for the excitation of the waves. This result agrees well with the findings of Barik et al. (2019c), where they have

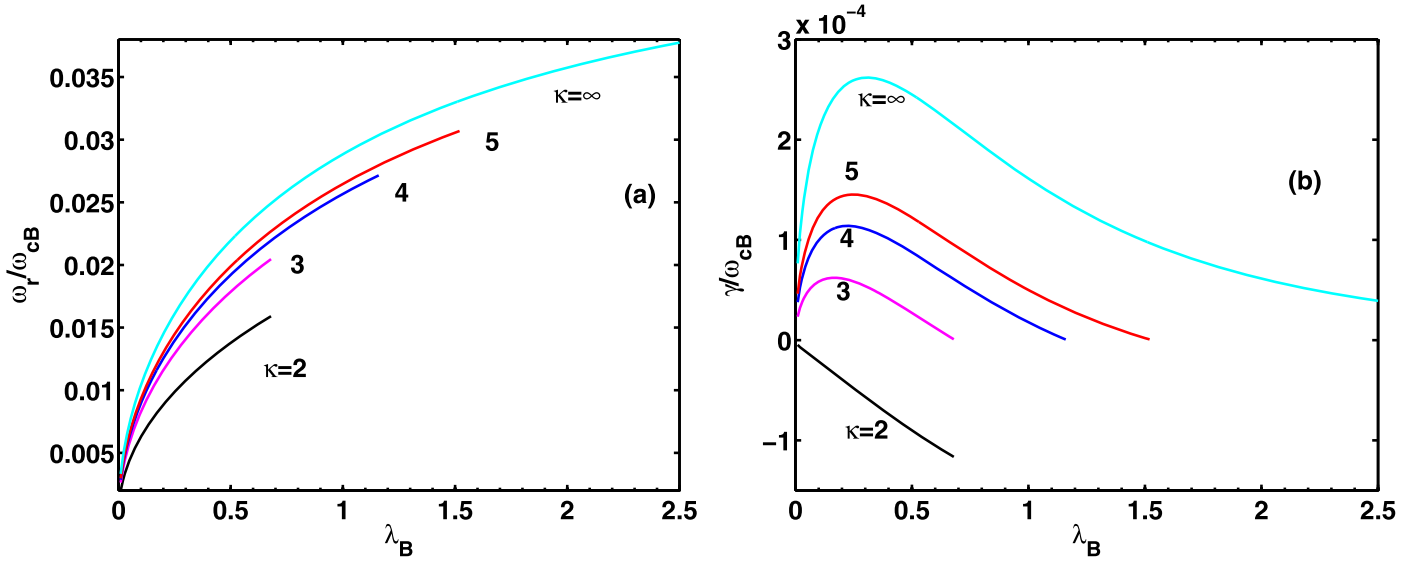

Figure 2. KAWs' resonant instability driven by ion beam: variation of (a) normalized real frequency, ω_r/ω_{cB}, and (b) normalized growth rate, γ/ω_{cB} vs. $\lambda_B = \frac{k_\perp^2 \alpha_B^2}{2\omega_{cB}^2}$ for $\frac{N_B}{N_e} = 0.18$, $\beta_i = 0.001$, $\theta = 87.14°$, $V_B/\alpha_B = 1.0$, $T_i/T_B = 0.016$, $T_e/T_B = 0.6$, and various values of κ as listed on the curves.

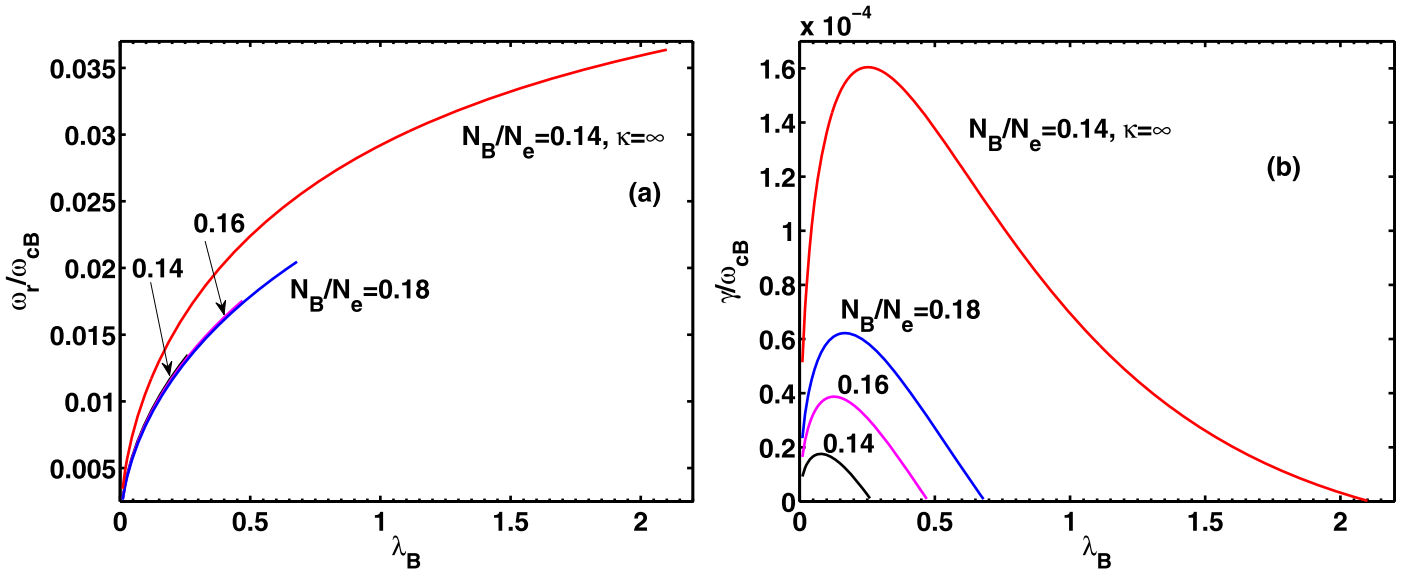

Figure 3. KAWs' resonant instability driven by ion beam: variation of (a) normalized real frequency, ω_r/ω_{cB}, and (b) normalized growth rate, γ/ω_{cB} vs. $\lambda_B = \frac{k_\perp^2 \alpha_B^2}{2\omega_{cB}^2}$ for $\beta_i = 0.001$, $\theta = 87.14°$, $V_B/\alpha_B = 1.0$, $T_i/T_B = 0.016$, $T_e/T_B = 0.6$, and various values of N_B/N_e as listed on the curves. All the curves are plotted for $\kappa = 3$ except the one that is for $\kappa = \infty$ as mentioned on the curve.

studied the effect of κ-electron with velocity shear as the source of free energy. However, the growth rate produced in their study is one order of magnitude larger than the results presented here. This indicates that the velocity shear is one of the more effective energy sources for the generation of KAWs as compared to the ion beam.

The ion beam number density effect on the real frequency and growth rate of KAWs for both Maxwellian as well as non-Maxwellian electrons is shown in Figure 3. For a non-Maxwellian electron ($\kappa = 3$ here), the peak growth rate increases with the increase in ion beam number density (N_B/N_e) and the corresponding real frequency also increases. For both cases, the wave unstable region increases with the increase in number density. The larger value of number density corresponds to a larger value of $\lambda_{B\,\max}$, i.e., the $\lambda_{B\,\max}$ shifts toward higher λ_B region with the increase in number density. For a fixed number density value $N_B/N_e = 0.14$, the result of non-Maxwellian electrons is compared with a Maxwellian one ($\kappa = \infty$). It is found that both the real frequency and growth rate are larger for Maxwellian electrons as compared to κ-electrons. Also, the wave unstable region is larger for Maxwellian electrons. A smaller ion beam number density can produce larger growth rate of KAWs in the presence of Maxwellian electrons, which is even higher than the growth rate produced by comparatively larger number density in the presence of non-Maxwellian electrons. This confirms that the presence of Maxwellian electrons favor the growth rate of KAWs, whereas non-Maxwellian electrons impede the KAWs' growth rate. From our numerics, it is observed that the growth rate of KAWs starts at a threshold value of ion beam number density ($N_B/N_e = 0.116$, for the plasma parameters considered here),

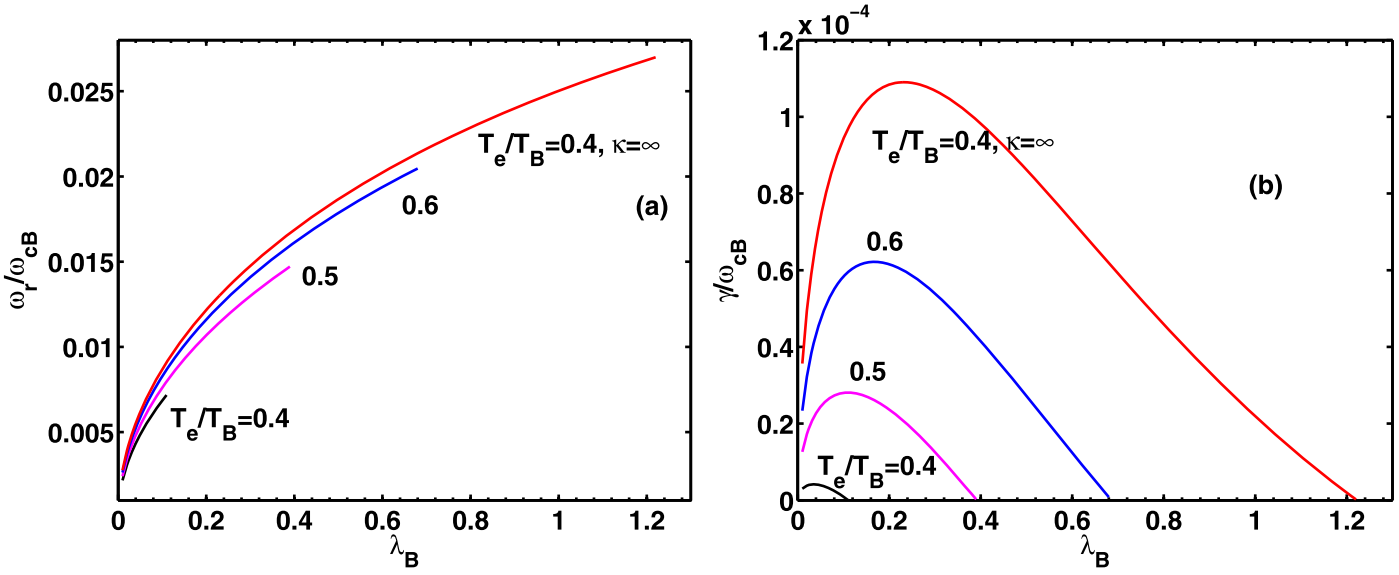

Figure 4. KAWs' resonant instability driven by ion beam: variation of (a) normalized real frequency, ω_r/ω_{cB}, and (b) normalized growth rate, γ/ω_{cB} vs. $\lambda_B = \frac{k_\perp^2 \alpha_B^2}{2\omega_{cB}^2}$ for $N_B/N_e = 0.18$, $\beta_i = 0.001$, $\theta = 87.14°$, $V_B/\alpha_B = 1.0$, and $T_i/T_B = 0.016$, $\kappa = 3$ for all the curves except the one that is for $\kappa = \infty$ and various values of T_e/T_B as listed on the curves.

increases further with the enhancement of number density. From the numerics, it is also found that at a larger value of ion beam velocity a smaller ion beam density can excite the KAWs, whereas a comparatively larger value of ion beam density is required to excite the waves at smaller ion beam velocity. This result agrees well with the findings of 2D hybrid simulation carried out by Hong et al. (2012), where they studied the generation of KAWs by an ion beam.

The temperature of the plasma species plays a key role in many plasma dynamics. The variation of the real frequency and growth rate of KAWs with λ_B for different electron temperatures T_e/T_B (which is normalized with respect to the beam ion temperature) at a fixed ion beam velocity $V_B/\alpha_B = 1.0$ for both Maxwellian and non-Maxwellian electrons is depicted in Figure 4. In the presence of non-Maxwellian electrons ($\kappa = 3$ here), the real frequency and growth rate both rise with the rise in electron temperature. The wave unstable region also increases as well. This confirms that the presence of hot non-Maxwellian electrons favors the growth of the KAWs. It is also observed that at smaller λ_B range the change in real frequency for different electron temperatures is negligible, whereas the growth rate changes significantly. However, both the real frequency and growth rate show significant changes at a higher λ_B range. A Maxwellian ($\kappa = \infty$) curve is drawn for the electron temperature $T_e/T_B = 0.4$ to compare the result with that of non-Maxwellian electrons. It is found that at the same temperature the presence of Maxwellian electrons can produce a comparatively larger real frequency and growth rate of KAWs for a larger wave unstable region λ_B as compared to non-Maxwellian electrons, which is even larger for the relatively high temperature of non-Maxwellian electrons. From the numerics, it is obtained that for the given set of plasma parameters the growth of the KAW starts at a threshold value of $T_e/T_B = 0.365$. Table 2 provides the threshold value of ion beam number density (N_B/N_e) and electron temperature (T_e/T_B) for electrons with different κ-values for the set of plasma parameters considered in Figures 3 and 4, respectively. From the table it is clear that the threshold value of number density varies inversely with the non-Maxwellian parameter κ, i.e., for smaller κ-electron the threshold is high and for larger κ (Maxwellian electron), the threshold value is small.

Table 2
Threshold Values of Ion Beam Number Density (Second Column) for $T_e/T_B = 0.6$ and Threshold Values of Electron Temperature for $N_B/N_e = 0.18$ at Different Values of κ

κ-parameter	Threshold Value of N_B/N_e	Threshold Value of T_e/T_B
3	0.116	0.365
4	0.097	0.297
5	0.089	0.267
∞	0.069	0.193

Note. Other common plasma parameters are $\beta_i = 0.001$, $\theta = 87.14°$, $V_B/\alpha_B = 1.0$, and $T_i/T_B = 0.016$.

The examination of the propagation angle effect on the growth of the wave is important as it allows exploring the regime of wave propagation. The variation of the real frequency and growth rate of KAWs with λ_B for different propagation angles at a fixed ion beam velocity $V_B/\alpha_B = 1.0$ is studied for both the Maxwellian and non-Maxwellian electrons and the results are described in Figure 5. It is observed that both the real frequency and growth rate of KAWs increase with the decrease in propagation angle in the presence of non-Maxwellian electrons ($\kappa = 3$ here), although the wave unstable region remains the same. It is also noted that at a fixed λ_B the changes in real frequency for different propagation angle are nominal at a smaller λ_B region, whereas the changes are significant at a larger λ_B region. However, the converse is true for the growth rate of KAWs, i.e., a significant changes in growth rate of KAWs is observed at a smaller λ_B region, while the changes are nominal at a larger λ_B. This observed trend is the same as the results obtained by Barik et al. (2019a). For comparison, a Maxwellian curve is plotted on the same figure. It is found that for the same propagation angle ($\theta = 89.5°$ here)

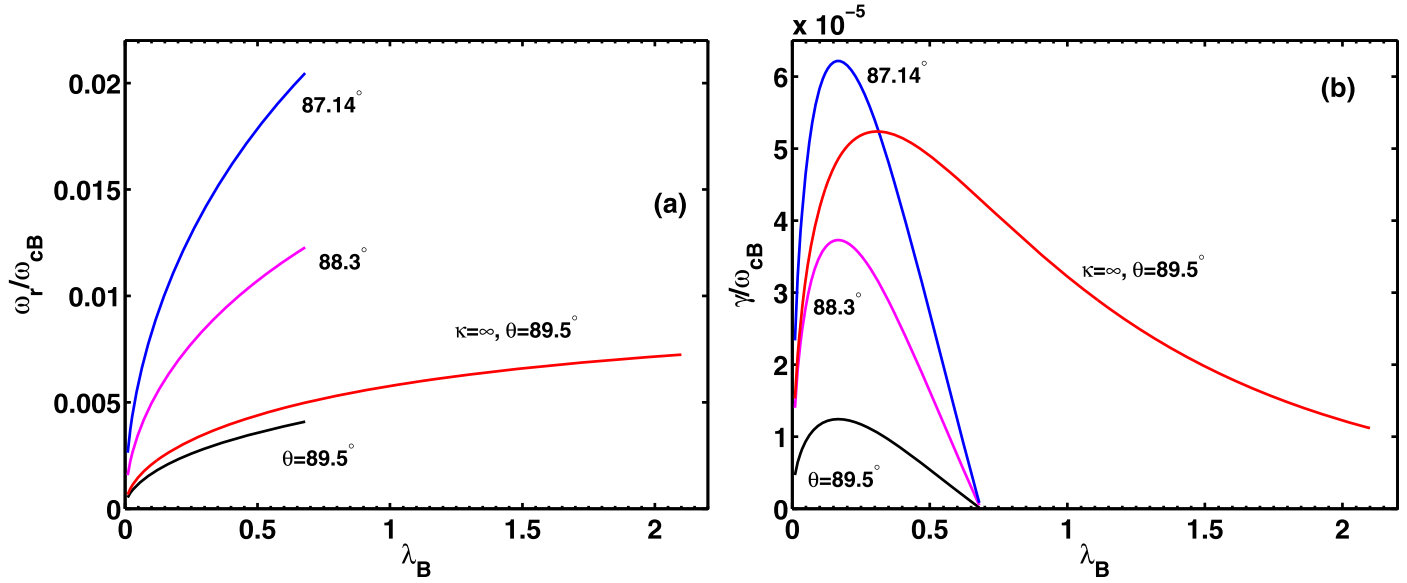

Figure 5. KAWs' resonant instability driven by ion beam: variation of (a) normalized real frequency, ω_r/ω_{cB}, and (b) normalized growth rate, γ/ω_{cB} vs. $\lambda_B = \frac{k_\perp^2 \alpha_B^2}{2\omega_{cB}^2}$ for $N_B/N_e = 0.18$, $\beta_i = 0.001$, $V_B/\alpha_B = 1.0$, $T_i/T_B = 0.016$, and $T_e/T_B = 0.6$, $\kappa = 3$ for all the curves except the one that is for $\kappa = \infty$ and various values of θ as listed on the curves.

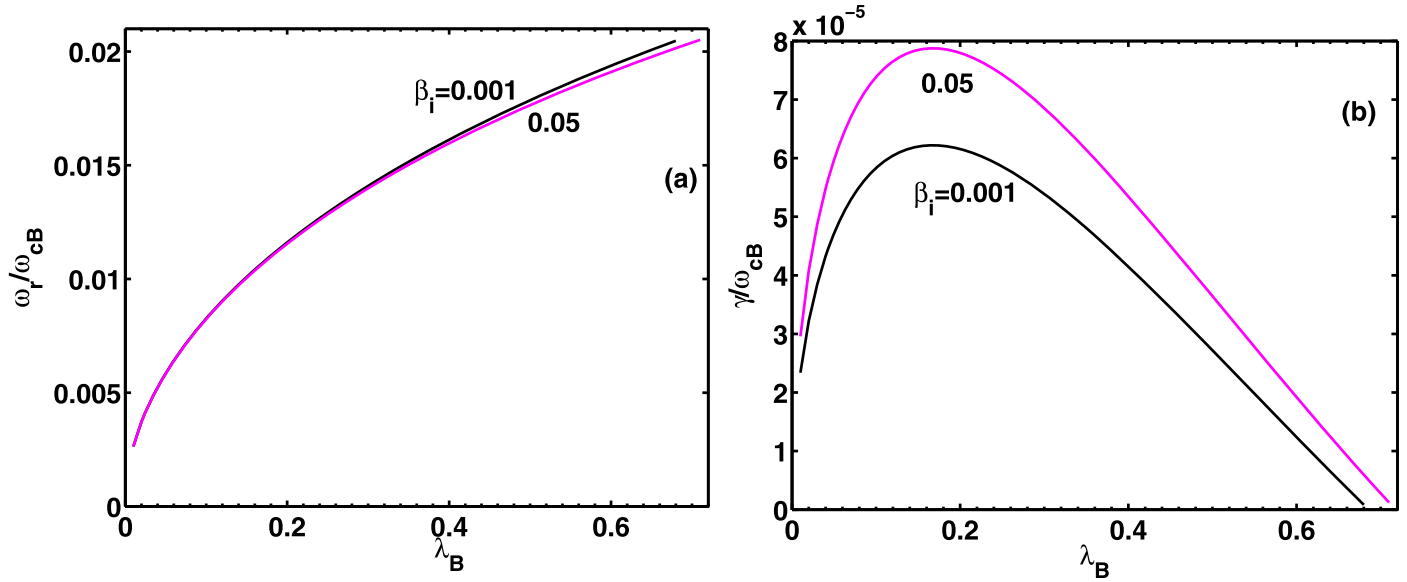

Figure 6. KAWs' resonant instability driven by ion beam: variation of (a) normalized real frequency, ω_r/ω_{cB}, and (b) normalized growth rate, γ/ω_{cB} vs. $\lambda_B = \frac{k_\perp^2 \alpha_B^2}{2\omega_{cB}^2}$ for $N_B/N_e = 0.18$, $\theta = 87.14°$, $V_B/\alpha_B = 1.0$, $T_i/T_B = 0.016$, $T_e/T_B = 0.6$, $\kappa = 3$, and various values of β_i as listed on the curves.

the presence of Maxwellian electrons in our model produces larger real frequency and growth rate as compared to non-Maxwellian electrons. This confirms the presence of Maxwellian electrons facilitates the growth rate of KAWs.

The plasma parameter β_i contains the information about the ion temperature T_i and ambient magnetic field B_0 in it. The effect of ion plasma beta (β_i) on the real frequency and growth rate of KAWs in the presence of non-Maxwellian electrons ($\kappa = 3$ here) is presented in Figure 6. It can be observed that the change in β_i parameter has a marginal effect on the real frequency, whereas the growth rate increases significantly with the increase in β_i value, and the unstable region extends to larger λ_B when β_i is increased.

6. Discussion and Conclusion

A theoretical model comprising of Maxwellian background ions and beam ions and κ-electrons is discussed to study the resonant instability of KAWs generated by ion beams. It is found that the presence of highly non-Maxwellian κ-electrons hinders the growth rate of KAWs by restricting the wave unstable region when ion beam velocity is considered as a free energy source, whereas a higher growth rate of KAWs is obtained as we approach the Maxwellian electrons. For a wave to grow, the slope of the particle distribution function near the phase velocity of the wave should be positive. Here, we used the κ-distribution function for electrons that are not drifting;

hence, no source of free energy is present out there. The slope of the κ-distribution function for electrons, near the phase velocity of the wave, is negative, which leads to the damping of the wave. The slope increases with the decrease in κ-parameter (high non-thermality), and as a consequence the κ-electron contribution to the wave damping increases when κ decreases. In the presence of κ-electrons the growth rate of the KAWs increases with the increase in ion beam velocity. It is worth mentioning that for κ-electrons, a high threshold value of ion beam velocity is required to excite the waves in comparison to Maxwellian electrons. The range of ion beam velocity (V_B/α_B) over which the growth rate of KAW is obtained increases as one approaches the κ- to Maxwellian electrons. The intensification of the ion beam increases the growth rate and real frequency of KAWs. At a fixed value of ion beam velocity a comparatively higher critical number density is required for κ-electrons to excite KAWs as compared to Maxwellian electrons. It is found that hot non-Maxwellian electrons favor the growth of KAWs' resonant instability driven by ion beam. It is also noted that for a fixed set of plasma parameters the threshold value of T_e/T_B is reciprocally related to the non-Maxwellian parameter κ, i.e., a high temperature threshold is required to excite KAWs for highly non-Maxwellian electron (smaller κ), whereas a comparatively smaller temperature threshold can generate wave growth for Maxwellian electrons. Both the real frequency and growth rate increase with the decrease in propagation angle. The β_i variation has a marginal effect on the real frequency of the KAWs. However, the growth rate increases with the increase in β_i value.

The ion beam alone as a source can excite KAWs for a significant growth rate, though it is smaller as compared to the case of KAWs generated by velocity shear. The outcomes of this model are able to verify few predictions of the 2D hybrid simulation done by Hong et al. (2012) such as (i) the power of the KAWs enhances due to enhancement in ion beam velocity and (ii) at a smaller value of ion beam velocity a larger value of ion beam number density is required to excite the KAWs and vice versa. In a two component electron-proton plasma as studied by Gary & Nishimura (2004), the inclusion of ion beam as a source of free energy gives rise to wave excitation rather than stabilization.

In order to show an application of our model, the plasma parameters relevant to the auroral field line/polar cusp region at an altitude of 5–7 R_E are considered (Lysak & Lotko 1996; Lakhina 2008; Barik et al. 2019a). The observed plasma parameters are ion beam densities $N_B/N_e = 0.01$–0.2 and ion beam speed $V_B/\alpha_B < 2$ (D'Angelo et al. 1974; Takada et al. 2005; Wygant et al. 2005). For our computational purposes, we have considered $N_B/N_e =$ 0.01–0.2 (see Table 2), $V_B/\alpha_B = 0.1$–2.05 (see Table 1), $\beta_i = 0.001$–0.05, ion beam cyclotron frequency $\omega_{cB}/2\pi \approx 2.2$–$3.0$ Hz, hot electron temperature $T_e \approx 100$ eV, the background cold ion temperature, $T_i \approx 10$ eV, and beam ion temperature $T_B \approx 1$–2 keV (D'Angelo et al. 1974; Gurnett & Frank 1978; Wygant et al. 2005).

For the parameters considered in Figure 4, the maximum normalized growth rate and the corresponding real frequency of KAWs are found to be 0.000062 and 0.0107, respectively, at $\lambda_B = 0.17$, whereas the wave is excited in the λ_B range of 0.01–0.68. The respective un-normalized growth rate and real frequency are 0.16 and 26.8 mHz, respectively. The ion beam driven resonant instability of KAWs can produce waves with frequencies up to ≈6.6–51.2 mHz and excite the wave up to a growth rate of ≈0.0021–0.16 mHz for the whole range of our computations. The perpendicular wavenumbers can be calculated using the relation $k_\perp = \sqrt{2\lambda_B}\,\omega_{cB}/\alpha_B$ and are found to be ≈0.0036–0.03 km^{-1} and the respective perpendicular wavelengths are $\lambda_\perp \approx 209$–$1745$ km. The parallel wavenumbers can be calculated from the relation $k_\parallel/k_\perp = 0.05$ and are obtained as ≈ 0.018–0.15×10^{-2} km^{-1} and the corresponding parallel wavelength are $\lambda_\parallel \approx 42$–$349 \times 10^2$ km.

The perpendicular wavelength of 209–1745 km that is obtained from this model lies in the upper limit of the observed values of 20–120 km in the polar region. The calculated value of the parallel wavelength 42–349×10^2 km matches well with the observed value of 1000–10,000 km (Wygant et al. 2002). This model can generate KAWs in the frequency range of 6.6–51.2 mHz, which may be able to explain the characteristics of the observed ULF waves of frequency 1 mHz–30 Hz. Though the model is applied to the plasma parameters of auroral region, it can also be applied to other regions as well to study the generation of KAWs where ion beam is found.

In this article, an application of the theoretical model to the auroral region of the Earth's magnetosphere is discussed. However, the model can be applied to solar corona, solar flare, solar wind, and planetary environments etc. as the observations indicate the presence of non-Maxwellian electrons, ion beams, and low beta plasma as mentioned in Section 1. It is also worth mentioning that this model can be applied to other astrophysical plasma where ion beams and relevant plasma environment are found.

G.S.L. thanks the Indian National Science Academy, New Delhi, for the support under the INSA-Honorary Scientist Scheme.

Appendix

The general expressions for number density and z-component of current density for jth plasma species with κ-distribution are given. Thereafter, the number density and z-component of current density for electrons are derived by expanding the modified plasma dispersion function (MPDF) in appropriate limit.

From Equation (9), after substituting the distribution function and solving the velocity integrals, the general expressions for perturbed number density and z-component of current density for jth species with κ-distribution are found.

Perturbed number density:

$$n_j = -\sum_{n=-\infty}^{+\infty} \frac{4e_jN_j}{m_j\Theta_j^2}\left(\frac{\omega_{cj}}{k_\perp\Theta_j}\right)^2 \left\{\left(\frac{n\omega_{cj}}{\omega}\right)\left[\left(\frac{n\omega_{cj}}{k_\parallel\Theta_j} + \chi_{nj}\right)K_1\right]\phi + \left[\left(\frac{n\omega_{cj}}{\omega}\chi_{nj} - \frac{\chi_{nj}^2}{\chi_0}\right)K_1 + \left(\frac{n\omega_{cj}}{\omega} + \frac{\chi_{nj}}{\chi_0}\right)K_2\right]\psi\right\} \tag{A1}$$

and z-component of perturbed current density:

$$J_{zj} = -\sum_{n=-\infty}^{+\infty} \frac{2e_j^2N_j}{m_j\theta_j}\left(\frac{\omega_{cj}}{k_\perp\theta_j}\right)^2 \times \left\{\left[\left(\frac{2n\omega_{cj}}{\omega}\chi_{nj}\chi_{0j}\right)K_1 + \left(\frac{2n\omega_{cj}}{\omega}\chi_{0j}\right)K_2\right]\phi + \left[\left\{2\chi_{nj}^2\left(\frac{n\omega_{cj}}{\omega} + \frac{\chi_{nj}}{\chi_{0j}}\right)\right\}K_1 + \left(\frac{2n\omega_{cj}}{\omega}\chi_{nj} + 2\frac{\chi_{nj}^2}{\chi_{0j}}\right)K_2\right]\psi\right\}. \tag{A2}$$

Equations (A1) and (A2) are the generalized perturbed number density and z-component of the current density, respectively, for a plasma species with κ-distribution without any approximations. Here, $\chi_{nj} = \frac{(\omega - n\omega_{cj})}{k_\parallel \Theta_j}$, $\chi_{0j} = \frac{\omega}{k_\parallel \Theta_j}$. The coefficients K_1 and K_2 that appears in Equations (A1) and (A2) have the following integral forms:

$$K_1 = \left(\frac{\kappa+1}{\kappa}\right)^{3/2}\left(\frac{\kappa-1/2}{\kappa}\right)\int_0^\infty \frac{\xi_j J_n^2(\xi_j)}{(1+\xi_j^2/2\lambda_j\kappa)^{\kappa+2}} \times Z^*_{\kappa+1}\left[\left(\frac{(\kappa+1)/\kappa}{1+\mu^2/2\lambda_j\kappa}\right)^{1/2}\chi_{nj}\right]d\xi_j, \tag{A3}$$

$$K_2 = \frac{(\kappa+1/2)(\kappa-1/2)}{\kappa^2}\int_0^\infty \frac{\xi_j J_n^2(\xi_j)d\xi_j}{(1+\xi_j^2/2\lambda_j\kappa)^{\kappa+3/2}}. \tag{A4}$$

Here, Z^*_κ is the modified plasma dispersion function (MPDF), which is given by Summers et al. (1994)

$$Z^*_\kappa(\zeta) = \frac{1}{\sqrt{\pi}}\frac{\Gamma(\kappa+1)}{\kappa^{3/2}\Gamma(\kappa-1/2)} \times\int_{-\infty}^{\infty}\frac{ds}{(s-\zeta)(1+s^2/\kappa)^{\kappa+1}}, \quad \mathrm{Im}(\zeta)>0, \tag{A5}$$

where s is any arbitrary variable. Equation (A5) is the MPDF of order κ and that of any desired order can be obtained by replacing parameters κ with the required order throughout the expression. To solve these integrals, it is necessary to expand the MPDF at a specific limit, which again depends upon the limit of argument λ_j. For $\lambda_j \to 0$, which is valid for κ electron species considered in this model, the MPDF needs to be expanded in the power series limit, which is given by Summers & Thorne (1991)

$$\begin{aligned} Z^*_\kappa(\zeta) &= \frac{\kappa!\sqrt{\pi}\,i}{\kappa^{3/2}\Gamma(\kappa-1/2)}\frac{1}{[1+(\zeta^2/\kappa)]^{\kappa+1}} \\ &- \frac{(2\kappa-1)(2\kappa+1)}{2\kappa^2} \times\zeta\left[1-\left(\frac{2\kappa+3}{2\kappa}\right)\zeta^2+\cdots\right],\ \zeta\to 0 \\ &= \frac{\kappa!\sqrt{\pi}\,i}{\kappa^{3/2}\Gamma(\kappa-1/2)}\left[1-\left(\frac{\kappa+1}{\kappa}\right)\zeta^2+\cdots\right] \\ &- \frac{(2\kappa-1)(2\kappa+1)}{2\kappa^2} \times\zeta\left[1-\left(\frac{2\kappa+3}{2\kappa}\right)\zeta^2+\cdots\right],\ \zeta\to 0. \end{aligned} \tag{A6}$$

The solution of the integrals in the limit $\lambda_e \to 0$ is given by

$$K_1 = \left\{\frac{1}{2^{|n|}}\frac{\kappa^{|n|}\Gamma(\kappa-|n|-1/2)}{\Gamma(|n|+1)\Gamma(\kappa-1/2)} \times\left(\frac{\kappa-|n|}{\kappa}\right)^{3/2}\lambda_e^{|n|+1} \times Z^*_{\kappa-|n|}\left[\left(\frac{\kappa-|n|}{\kappa}\right)^{1/2}\chi_{ne}\right]+\cdots\right\}, \tag{A7}$$

$$K_2 = \left\{\frac{1}{2^{|n|}}\frac{\kappa^{|n|-1}\Gamma(\kappa-|n|+1/2)}{\Gamma(|n|+1)\Gamma(\kappa-1/2)}\lambda_e^{|n|+1}+\cdots\right\}. \tag{A8}$$

Here, K_1 is valid for the condition $\kappa > |n| + \frac{1}{2}$, whereas, K_2 is valid for $\kappa > |n| - \frac{1}{2}$. Here, $\lambda_e = \frac{1}{2}\frac{k_\perp^2\Theta_e^2}{\omega_{ce}^2}$ and $\Theta_e = \left[\left(\frac{\kappa-3/2}{\kappa}\right)\right]^{1/2}\left(\frac{2T_e}{m_e}\right)^{1/2}$ is the modified thermal speed of electrons. To arrive at Equations (A7) and (A8), following identities are used:

$$\begin{aligned} &\int_0^\infty \frac{x^{\rho-1}J_\mu(cx)J_\nu(cx)dx}{(ax^2+b^2)^{\lambda+1}} = \frac{c^{2\lambda+2-\rho}}{2\sqrt{\pi}a^{\lambda+1}}\left(\frac{c^2b^2}{a}\right)^{[(\mu+\rho+\nu)/2-\lambda-1]} \\ &\times\frac{\Gamma[(\rho+\mu+\nu)/2]\Gamma[\lambda+1-(\rho+\mu+\nu)/2]\Gamma[(\mu+\nu+1)/2]\Gamma[1+(\mu+\nu)/2]}{\Gamma[\lambda+1]\Gamma[\mu+\nu+1]\Gamma[\mu+1]\Gamma[\nu+1]} \\ &\times{}_3F_4\Big(\tfrac{1}{2}(\rho+\mu+\nu),\ \tfrac{1}{2}(\mu+\nu+1),\ \tfrac{1}{2}(\mu+\nu)+1; \\ &\tfrac{1}{2}(\rho+\mu+\nu)-\lambda,\ \mu+\nu+1,\ \mu+1,\ \nu+1;\ \tfrac{c^2b^2}{a}\Big)+\frac{c^{2\lambda+2-\rho}}{2\sqrt{\pi}a^{\lambda+1}} \\ &\times\frac{\Gamma[(\mu+\nu+\rho)/2-\lambda-1]\Gamma[\lambda+3/2-\rho/2]\Gamma[\lambda+2-\rho/2]}{\Gamma[\lambda+2+(\mu+\nu-\rho)/2]\Gamma[\lambda+2-(\rho-\mu+\nu)/2]\Gamma[\lambda+2-(\rho+\mu-\nu)/2]} \times{}_3F_4 \\ &\Big(\lambda+1,\ \lambda+\tfrac{3}{2}-\tfrac{1}{2}\rho,\ \lambda+2-\tfrac{1}{2}\rho,\ \lambda+2 \\ &-\tfrac{1}{2}(\rho-\mu-\nu),\ \lambda+2-\tfrac{1}{2}(\rho+\mu-\nu), \\ &\lambda+2-\tfrac{1}{2}(\rho-\mu+\nu),\ \lambda+2-\tfrac{1}{2}(\rho+\mu+\nu),\ \tfrac{c^2b^2}{a}\Big), \end{aligned} \tag{A9}$$

where $-(\mu+\nu) < \rho < 2\lambda + 7/2$, ${}_3F_4$ is the hypergeometric series given by

$$\begin{aligned} &{}_3F_4[\alpha_1,\alpha_2,\alpha_3;\beta_1,\beta_2,\beta_3,\beta_4;z] \\ &= \sum_{p=0}^\infty \frac{(\alpha_1)_p,(\alpha_2)_p,(\alpha_3)_p}{(\beta_1)_p,(\beta_2)_p,(\beta_3)_p,(\beta_4)_p}\frac{z^p}{p!} \end{aligned} \tag{A10}$$

and

$$(\alpha)_p = \frac{\Gamma(\alpha+p)}{\Gamma(\alpha)} \tag{A11}$$

$$\int_0^\infty x J_n^2(x)e^{-x^2/(2\lambda)}dx = \lambda b_n, \tag{A12}$$

where $\lambda > 0$, $n = 0, \pm1, \pm2, \pm3, \cdots$ and $b_n = e^{-\lambda}I_n(\lambda)$, I_n is the modified Bessel function.

With the substitution of solutions of the integrals K_1 and K_2 from Equations (A7) and (A8) in Equations (A1) and (A2) and replacing the jth symbol by the electron's expression, the perturbed number density and z-component of the current density for the electrons can be evaluated and are given by: the perturbed electron number density

$$n_e = \sum_{n=-\infty}^{+\infty}\frac{4eN_e}{m_e\Theta_e^2}\left(\frac{\omega_{ce}}{k_\perp\Theta_e}\right)^2\left\{\left(\frac{n\omega_{ce}}{\omega}\right)\left[\left(\frac{n\omega_{ce}}{k_\parallel\Theta_e}+\chi_{ne}\right)K_1\right]\phi + \left[\left(\frac{n\omega_{ce}}{\omega}\chi_{ne}-\frac{\chi_{ne}^2}{\chi_{0e}}\right)K_1+\left(\frac{n\omega_{ce}}{\omega}+\frac{\chi_{ne}}{\chi_{0e}}\right)K_2\right]\psi\right\} \tag{A13}$$

and the z-component of perturbed electron current density

$$J_{ze} = -\sum_{n=-\infty}^{+\infty} \frac{2e^2 N_e}{m_e \Theta_e}\left(\frac{\omega_{ce}}{k_\perp \Theta_e}\right)^2 \times \left\{\left[\left(\frac{2n\omega_{ce}}{\omega}\chi_{ne}\chi_{0e}\right)K_1 + \left(\frac{2n\omega_{ce}}{\omega}\chi_{0e}\right)K_2\right]\phi + \left[2\chi_{ne}^2\left(\frac{n\omega_{ce}}{\omega} + \frac{\chi_{ne}}{\chi_{0e}}\right)K_1 + \left(\frac{2n\omega_{ce}}{\omega}\chi_{ne} + 2\frac{\chi_{ne}^2}{\chi_{0e}}\right)K_2\right]\psi\right\}, \quad \text{(A14)}$$

where $\chi_{ne} = \frac{(\omega - n\omega_{ce})}{k_\parallel \Theta_e}$, $\chi_{0e} = \frac{\omega}{k_\parallel \Theta_e}$

Under the assumption of low frequency, i.e., $\omega \ll \omega_{ce}$ and long parallel wavelength, i.e., $k_\parallel \Theta_e \ll \omega_{ce}$, the MPDF will have a large argument $|(\omega - n\omega_{ce})/k_\parallel \Theta_e| \gg 1$ for $n \neq 0$ (Lysak & Lotko 1996), hence, expanded in the asymptotic limit as mentioned in Summers & Thorne (1991). Since the leading order terms have the dominant contribution, Equations (A13) and (A14) are simplified further for $n = \pm 1$ to arrive at Equations (14) and (15). Also, with this approximation the higher order terms of λ_e (which is small, i.e., $\lambda_e \to 0$) that appears in the expressions of K_1 and K_2 are neglected.

ORCID iDs

K. C. Barik https://orcid.org/0000-0003-3958-4587
S. V. Singh https://orcid.org/0000-0003-2758-7713
G. S. Lakhina https://orcid.org/0000-0002-8956-486X

References

Artemyev, A. V., Zimovets, I. V., & Rankin, R. 2016, A&A, 589, A101
Astfalk, P., Görler, T., & Jenko, F. 2015, JGRA, 120, 7107
Barik, K. C., Singh, S. V., & Lakhina, G. S. 2019a, PhPl, 26, 022901
Barik, K. C., Singh, S. V., & Lakhina, G. S. 2019b, URSI Radio Science Bulletin, 2019, 17
Barik, K. C., Singh, S. V., & Lakhina, G. S. 2019c, PhPl, 26, 112108
Barik, K. C., Singh, S. V., & Lakhina, G. S. 2020, ApJ, 897, 172
Bellan, P. M. 2015, Fundamentals of Plasma Physics (Cambridge: Cambridge Univ. Press)
Boehm, M. H., Carlson, C. W., McFadden, J. P., Clemmons, J. H., & Mozer, F. S. 1990, JGR, 95, 12157
Chaston, C. C., Bonnell, J. W., Clausen, L., & Angelopoulos, V. 2012, JGRA, 117, A09202
Chaston, C. C., Bonnell, J. W., Wygant, J. R., et al. 2018, GeoRL, 45, 2128
Chaston, C. C., Peticolas, L. M., Carlson, C. W., et al. 2005, JGRA, 110, A02211
Chen, L., & Hasegawa, A. 1974, JGR, 79, 1024
D'Angelo, N. 1973, JGR, 78, 1206
D'Angelo, N. 1977, RvGeo, 15, 299
D'Angelo, N., Bahnsen, A., & Rosenbauer, H. 1974, JGR, 79, 3129
Delamere, P. A., Ng, C. S., Damiano, P. A., et al. 2021, JGRA, 126, e28479
Duan, S., Dai, L., Wang, C., et al. 2017, JGRA, 122, 11,256
Duan, S., Liu, Z., & Angelopoulos, V. 2012, ChSBu, 57, 1429
Futaana, Y., Machida, S., Saito, Y., Matsuoka, A., & Hayakawa, H. 2003, JGRA, 108, 1025
Gaelzer, R., & Ziebell, L. F. 2014, JGRA, 119, 9334
Gary, G. A. 2001, SoPh, 203, 71
Gary, S. P. 1986, JPlPh, 35, 431
Gary, S. P., & Nishimura, K. 2004, JGRA, 109, A02109
Gershman, D. J., F-Viñas, A., Dorelli, J. C., et al. 2017, NatCo, 8, 14719
Goertz, C. K., & Boswell, R. W. 1979, JGR, 84, 7239
Goldstein, B. E., Neugebauer, M., Zhou, X.-Y., et al. 2010, in AIP Conf. Proc. 1216, Twelfth Int. Solar Wind Conf., ed. M. Maksimovic et al. (Melville, NY: AIP), 261
Grison, B., Sahraoui, F., Lavraud, B., et al. 2005, AnGeo, 23, 3699
Gurnett, D. A., & Frank, L. A. 1978, JGR, 83, 1447
Hasegawa, A. 1976, JGR, 81, 5083
Hasegawa, A., & Chen, L. 1976, PhFl, 19, 1924
Hasegawa, A., & Mima, K. 1978, JGR, 83, 1117
Hollweg, J. V. 1999, JGR, 104, 14811
Hong, M. H., Lin, Y., & Wang, X. Y. 2012, PhPl, 19, 072903
Huba, J. D. 1981, JGR, 86, 8991
Hui, C. H., & Seyler, C. E. 1992, JGR, 97, 3953
Iwai, K., Shibasaki, K., Nozawa, S., et al. 2014, EP&S, 66, 149
Johnson, J. R., Cheng, C. Z., & Song, P. 2001, GeoRL, 28, 227
Keiling, A., Parks, G. K., Wygant, J. R., et al. 2005, JGRA, 110, A10S11
Keiling, A., Wygant, J. R., Catell, C., et al. 2002, JGRA, 107, 1132
Keiling, A., Wygant, J. R., Cattell, C., et al. 2000, GeoRL, 27, 3169
Keiling, A., Wygant, J. R., Cattell, C., et al. 2001, JGRA, 106, 5779
Lakhina, G. 2008, AdSpR, 41, 1688
Lakhina, G. S. 1987, JGR, 92, 12161
Lakhina, G. S. 1990, Ap&SS, 165, 153
Lazar, M., Fichtner, H., & Yoon, P. H. 2016, A&A, 589, A39
Leblanc, F., Chaufray, J. Y., Modolo, R., et al. 2017, JGRE, 122, 2401
Livadiotis, G. 2015, JGRA, 120, 880
López, R. A., Lazar, M., Shaaban, S. M., et al. 2019, ApJL, 873, L20
Louarn, P., Wahlund, J. E., Chust, T., et al. 1994, GeoRL, 21, 1847
Lysak, R. L., & Carlson, C. W. 1981, GeoRL, 8, 269
Lysak, R. L., & Dum, C. T. 1983, JGR, 88, 365
Lysak, R. L., & Lotko, W. 1996, JGRA, 101, 5085
Malara, F., Nigro, G., Valentini, F., & Sorriso-Valvo, L. 2019, ApJ, 871, 66
Marsch, E., Mühlhäuser, K.-H., Schwenn, R., et al. 1982, JGR, 87, 52
Meziane, K., Wilber, M., Hamza, A. M., et al. 2007, JGRA, 112, n/a
Moya, P. S., Gallo-Méndez, I., & Zenteno-Quinteros, B. 2021, JASTP, 219, 105630
Moya, P. S., Pinto, V. A., Viñas, A. F., et al. 2015, JGRA, 120, 5504
Narita, Y., Roberts, O. W., Vörös, Z., & Hoshino, M. 2020, FrP, 8, 166
Nosé, M., Iyemori, T., Sugiura, M., et al. 1998, JGR, 103, 17587
Parks, G., Chen, L. J., McCarthy, M., et al. 1998, GeoRL, 25, 3285
Pierrard, V., & Lazar, M. 2010, SoPh, 267, 153
Procházka, O., Reid, A., Milligan, R. O., et al. 2018, ApJ, 862, 76
Rathore, B. S., Gupta, D. C., & Kaushik, S. C. 2015, RAA, 15, 85
Salem, C. S., Howes, G. G., Sundkvist, D., et al. 2012, ApJL, 745, L9
Schriver, D., Ashour-Abdalla, M., Collin, H., & Lallande, N. 1990, JGR, 95, 1015
Sergis, N., Jackman, C. M., Masters, A., et al. 2013, JGRA, 118, 1620
Sharma, R. P., Goyal, R., Scime, E. E., & Dwivedi, N. K. 2014, PhPl, 21, 042113
Sharma, R. P., & Modi, K. V. 2013, PhPl, 20, 082305
Simnett, G. M. 1995, SSRv, 73, 387
Summers, D., & Thorne, R. M. 1991, PhFlB, 3, 1835
Summers, D., Xue, S., & Thorne, R. M. 1994, PhPl, 1, 2012
Takada, T., Seki, K., Hirahara, M., et al. 2005, JGRA, 110, A02204
Thompson, B. J., & Lysak, R. L. 1996, JGRA, 101, 5359
Vasyliunas, V. M. 1968, JGR, 73, 7519
Wahlund, J.-E., Louarn, P., Chust, T., et al. 1994, GeoRL, 21, 1831
Wang, H., Lin, Y., Wang, X., & Guo, Z. 2019, PhPl, 26, 072102
Wygant, J. R., Cattell, C. A., Lysak, R., et al. 2005, JGRA, 110, A09206
Wygant, J. R., Keiling, A., Cattell, C. A., et al. 2002, JGRA, 107, 1201
Zastrow, M. 2016, Eos, 97